Biophysical Journal
Article

Biophysical Society

Circular Dichroism Spectroscopy of Collagen Fibrillogenesis: A New Use for an Old Technique

Kathryn E. Drzewiecki,[1] Daniel R. Grisham,[1] Avanish S. Parmar,[2] Vikas Nanda,[3] and David I. Shreiber[1,*]
[1]Department of Biomedical Engineering, Rutgers, The State University of New Jersey, Piscataway, New Jersey; [2]Department of Physics, Indian Institute of Technology, Banaras Hindu University, Varanasi, Uttar Pradesh, India; and [3]Center for Advanced Biotechnology and Medicine, Department of Biochemistry and Molecular Biology, Rutgers, The State University of New Jersey, Piscataway, New Jersey

ABSTRACT Type-I collagen assembles in a stepwise, hierarchic fashion from the folding of the triple helix to the assembly of fibrils into fibers. The mature assembled fibers are crucial for tissue structure and mechanics, cell interactions, and other functions in vivo. Although triple helix folding can be followed with the use of optical methods such as circular dichroism (CD) spectroscopy, fibrillogenesis is typically measured by alternative methods such as turbidity, rheology, and microscopy. Together, these approaches allow for investigation of the mechanical properties and architectures of collagen-based scaffolds and excised tissues. Herein, we demonstrate that CD spectroscopy, a technique that is used primarily to evaluate the secondary structure of proteins, can also be employed to monitor collagen fibrillogenesis. Type-I collagen suspensions demonstrated a strong, negative ellipticity band between 204 and 210 nm under conditions consistent with fibrillogenesis. Deconvolution of CD spectra before, during, and after fibrillogenesis identified a unique fibril spectrum distinct from triple helix and random coil conformations. The ability to monitor multiple states of collagen simultaneously in one experiment using one modality provides a powerful platform for studying this complex assembly process and the effects of other factors, such as collagenases, on fibrillogenesis and degradation.

INTRODUCTION

Type-I collagen is widely studied for many biomedical applications. It is a major component of scaffolds for tissue engineering (1,2) and in vitro cell substrates for studying cell adhesion (3), migration (4), and differentiation (5). Many implantable materials that are commonly used for the treatment of burns (6) and scars (7) are collagen based. Cosmetic companies produce a variety of collagen creams and injections as anti-aging treatments (8). In addition to its widespread use and continued development as a biomaterial throughout the biotechnology and cosmetics sectors, collagen is also studied to better understand how mutations in structure or synthesis lead to diseases such as Ehlers-Danlos syndrome and osteogenesis imperfecta (9,10). Given its extensive presence throughout the body, roles in various pathologies, and potential therapeutic uses, it is necessary to study the structure, functions, and interactions of collagen.

The 29 members of the collagen family in animals account for ~30% of the total body protein content (11). Type-I collagen (herein referred to as collagen unless otherwise stated) is composed of two α1 chains and one α2 chain, which associate into a right-handed triple helix (11). These helices further assemble through fibrillogenesis into highly organized fibrils with an evident D-periodic banding every 67 nm along the axis (Fig. S1 A in the Supporting Material). This higher-order structure produces fibers much longer than a single monomer (12), supporting tissues with various mechanical properties throughout the body (13).

Collagen assembly in vivo is tightly regulated by the cell (14–16). However, many of the structural and functional features of assembled fibrils can be recreated in vitro under appropriate conditions using collagen extracted from a variety of source animal tissues into neutral salt or buffers, or, more frequently, into dilute acidic solutions (1). Fibrillogenesis can be controlled by varying the pH (17–20), temperature (18,19,21,22), and buffer conditions (17,18,23,24). Under acidic conditions, collagen exists primarily as a soluble triple helix (17) below its melting transition around 42°C (24). At neutral pH, collagen readily forms fibrils above 20°C (17). The various stages of collagen assembly can be isolated and studied independently by manipulating the solution conditions.

Investigators have studied the soluble triple helix and fibril stages of collagen self-assembly using a variety of

Submitted May 23, 2016, and accepted for publication October 19, 2016.
*Correspondence: shreiber@soe.rutgers.edu
Editor: Elizabeth Rhoades.
http://dx.doi.org/10.1016/j.bpj.2016.10.023

experimental methods. Circular dichroism (CD) spectroscopy is a powerful tool for studying the folding of collagen and other model triple-helical peptide systems (25). CD spectroscopy measures the difference in the absorption of left-handed and right-handed circularly polarized light by the ensemble of peptide bond chromophores in a protein (26). In the case of the triple helix, the unique supercoiled polyproline type II secondary structure of the protein backbone exhibits distinct CD transitions, including a positive band at 222 nm and a negative band at 195 nm (26).

A number of scattering and mechanical methods have been used to investigate fibril formation during self-assembly. When fibrils are incubated at physiological pH and temperature, typical fibrillogenesis proceeds through an initial lag phase, rapid growth of collagen fibrils, and a plateau phase during which the collagen fibrils mature and stabilize (27,28). Depending on the technique utilized, some or all of these phases may be captured. After the growth phase, transmission electron microscopy or atomic force microscopy (AFM) can be used to image the collagen fibril structure, notably the characteristic D-banding of fibrils based on the stagger between collagen segments (Fig. S1 A) (12). At higher collagen concentrations, as the collagen self-assembles into a fibrillar hydrogel, rheological properties can be monitored to capture changes in the storage modulus that coincide with the transition from a liquid suspension to a semisolid hydrogel (Fig. S1 B). Optical measurements can also be used to study fibrillogenesis and structure. By assessing light scattering or turbidity, one can follow self-assembly via changes in the optical density of a low-concentration collagen solution during the lag, growth, and plateau phases (29). The structure of fibrils can also be observed by second-harmonic-generation light microscopy (30–32).

Although these powerful methods can be used to study either the triple helix or fibril state of collagen, few approaches allow concurrent observation of folding and higher-order assembly. Such studies generally rely on scattering approaches (33) to observe species over a wide range of size scales. Herein, we describe the observation of fibrillogenesis using CD spectroscopy under conditions in which both triple helix and fibril states can be observed simultaneously. Previously, a unique CD spectrum was observed during temperature-induced self-assembly of a chemically modified collagen derivative that was coincident with fibrillogenesis and distinct from that of a triple helix (24). Here, we establish the spectral shape of this component and demonstrate its utility for studying hierarchic assembly. As collagen solutions are most often analyzed under conditions in which fibrillogenesis is inhibited (19,34–42), this signal has not previously been extensively described or studied. However, given the wide accessibility of CD spectroscopy, the identification of a collagen-fibril-associated spectrum presents opportunities to study collagen fibrillogenesis and associated structural transitions in solution.

MATERIALS AND METHODS

Materials

Experiments were performed with collagen from multiple sources and vendors. Type-I collagen extracted from bovine skin (C857, Telo-EPC) was obtained from Elastin Products (Owensville, MO). Separate solutions of bovine skin-derived type-I collagen with and without telopeptides (TeloCol #5026-D (Telo-ABM) and PureCol #5005-B (Atelo-ABM)) were obtained from Advanced BioMatrix (Carlsbad, CA). Rat-tail type-I collagen (CB354249, RT) was obtained from Thermo Fisher Scientific (Waltham, MA). Human type-III collagen (#5021, type-III) was purchased from Advanced BioMatrix. Gelatin (G-9391) was purchased from Sigma-Aldrich (St. Louis, MO). All other materials were purchased from Sigma-Aldrich unless otherwise stated.

CD

CD spectra were obtained using an Aviv model 400 spectrometer (Aviv Biomedical, Lakewood, NJ). All samples were prepared to a final concentration of 0.1 mg/mL unless otherwise stated. Table 1 provides details regarding sample preparation and nomenclature. Samples (300 μL) were loaded into optically matched quartz cuvettes (0.1 cm path length; model 110-OS, Hellma USA, Plainview, NY). All ellipticity measurements were performed using the same cuvette for baselines and samples. Ellipticity measurements were corrected for buffer baseline, and when possible, ellipticity was converted to mean residue ellipticity (MRE) using sequence lengths for type-I and type-III collagen as identified in UniProtKB (Table 1) and molecular weights provided by the manufacturers. Data were excluded

TABLE 1 Collagen Sample Preparations

Sample Name	Type	Source	Buffer	pH	UniProtKB Sequence	Manufacturer
Telo-EPC	type-I collagen	bovine	0.02 M AcA	4	P02453, P02465	Elastin Products
			PBS	7		
			PBS and 1 M glycerol	7		
Telo-ABM	type-I collagen	bovine	0.01 M HCl	2	P02453, P02465	Advanced BioMatrix
			PBS	7		
Atelo-ABM	type-I collagen (no telopeptides)	bovine	0.01 M HCl	2	P02453, P02465 (no telopeptides)	Advanced BioMatrix
			PBS	7		
RT	type-I collagen	rat	0.02 M AcA	4	P02454, P02466	Thermo Fisher Scientific
			PBS	7		
Type-III	type-III collagen	human	0.01 M HCl	2	P02461	Advanced BioMatrix
			PBS	7		
Gelatin	denatured collagen	bovine	PBS	7	N/A	Sigma-Aldrich

Description of collagens, manufacturers, types, sources, buffers, sample pH for experiments, and UniProtKB references for MRE approximations.

from analysis if the dynode voltage exceeded 600 V, which is an issue primarily for ellipticities recorded at shorter wavelengths. For clarity, error bars are not shown for CD measurements; however, the maximum machine percent error obtained was an error of 8%, and the average instrument percent error was ~2.5% in the peak wavelength regions (220–225 nm or 198–210 nm).

The experiments are described in brief, and additional experimental parameters for CD are outlined in Table S1. The triple-helical content of all samples was confirmed via wavelength scans at 4°C (Table S1, experiment 1; Fig. S2). Folding and assembly of samples were monitored via the ellipticity at 222 nm, where a positive band coincides with triple helix structure. Structural changes at 222 nm were measured as the temperature was raised from 4°C to 60°C at a slow rate of 0.1°C/min to minimize kinetic effects, as described in Persikov et al. (43).

Separately, the total secondary structure change in response to increasing temperature was captured by collecting wavelength spectra from 4°C to 60°C (Table S1, experiment 2).

The digestion kinetics was observed by following changes in the CD spectrum of collagen upon addition of type-I collagenase (Table S1, experiment 3). Before digestion, ellipticity was monitored at 4°C and 37°C to confirm triple-helical and fibril content, respectively. Then, type-I collagenase or buffer was added to each cuvette and wavelength scans were performed over the course of the digest.

Rheology

The mechanical properties of collagen hydrogels were characterized for the above-described samples. Telo-EPC was mixed in 500 μL batches containing 10 μL 1 M HEPES, 65 μL 0.15 M NaOH, 50 μL 10× phosphate-buffered saline (PBS), 36.5 μL 1× PBS (Thermo Fisher Scientific), and 338.5 μL Telo-EPC (3.75 mg/mL, solubilized in 0.02 N acetic acid (AcA)) to create a 2.5 mg/mL collagen suspension. In separate samples of Telo-EPC, the 1× PBS was replaced with 36.5 μL of 13.7 M glycerol to prevent self-assembly (37), for a final concentration of 1 M glycerol in the buffered collagen sample. Telo-ABM and Atelo-ABM (Advanced BioMatrix) batches were prepared according to the manufacturer's protocols. Briefly, 400 μL of Telo-ABM (3.1 mg/mL) were mixed with 50 μL of 10× PBS and 61 μL of 0.1 M NaOH, and 400 μL of Atelo-ABM (3.1 mg/mL) was mixed with 50 μL of 10× PBS and 62 μL of 0.1 M NaOH to create 2.4 mg/mL suspensions. RT samples were diluted from 10 mg/mL to 3.75 mg/mL in 0.02 N AcA and were buffered according to the formula for Telo-EPC to prepare a collagen suspension at a final concentration of 2.5 mg/mL. Acid-buffered samples were also tested to confirm their inability to self-assemble by diluting the samples in acid (AcA or hydrochloric acid (HCl); see Table 1) to the final concentrations as outlined above.

Temperature-dependent mechanical properties were assessed using a Kinexus Ultra rotational rheometer (Malvern Instruments, Malvern, UK). A 200 μl sample was loaded into a 600 μm gap between 20 mm-diameter parallel plates. The bottom plate was connected to a Peltier temperature-controlled stage. To acquire the fibrillogenesis profile, the temperature was raised from 4°C to 60°C at a rate of 1°C/min. The sample was continually oscillated to 0.5% strain at 1 rad/s while the resultant torque was measured to obtain the temperature-dependent sample storage modulus (G′).

Independent component analysis

The CD spectral component associated with the collagen fibril was determined from a data set of 60 experimental CD spectra for 0.1 mg/mL Telo-EPC (Table S1, experiment 2). Reconstruction of all 60 spectra was attempted using a mixture of constrained triple helix and random coil spectra plus a third, unconstrained component associated with the assembled fibril. The fast independent component analysis (fastICA) algorithm was used (44–46) to determine the unconstrained component and the weights of the three components as a function of temperature. A χ^2 analysis indicated that three components were sufficient to determine the series of experimental spectra. Considering each CD spectrum as a linear combination of component spectra, the component spectra were fit to Eq. 1 using error-weighted multiple regression to determine the fractional population of each component with changing temperature:

$$X_T = f_H(T)H + f_F(T)F + f_M(T)M, \quad (1)$$

where X_T is the measured spectrum at temperature T, and H, F, and M correspond to the fitted component spectra corresponding to the triple helix, fibril, and random coil (heat-denatured collagen), respectively. The fractions of signal corresponding to these spectral components are $f_H(T)$, $f_F(T)$, and $f_M(T)$, respectively.

To evaluate the distributions of the independent components as collagen was enzymatically degraded, the components were fit using the same approach as described above on a set of 66 experimental CD spectra taken over several hours for the same collagen sample treated with type-I collagenase at a constant temperature of 37°C (Table S1, experiment 3). Three-variable regression with all components was applied across the entire data set. The source code, installation instructions, and sample input/output files are provided in Supporting Materials and Methods.

RESULTS

CD signal change associated with fibrillogenesis

Heating of a triple-helical solution of type-I collagen (Telo-EPC) at pH 7 resulted in two transitions in the rheological properties: an increase in the storage modulus (G′) at 30°C, consistent with fibrillogenesis and formation of a hydrogel, and a return to a G′ of ~0 at 50°C, associated with collagen denaturation (Fig. 1 *A*). Performing the same experiment in a CD spectrometer also showed two transitions that coincided with the shifts in G′ upon fibrillogenesis and denaturation. A large increase in the negative amplitude of the MRE at 222 nm upon fibrillogenesis has not been described before, to our knowledge, which motivated us to further investigate this phenomenon. The dynode voltage of the CD spectrometer is an instrument parameter that increases with elevations in the optical density of a sample. The dynode voltage did not significantly change during the course of temperature profile experiments (Fig. S3). This indicates that the large negative MRE obtained under conditions of fibrillogenesis is likely not a trivial result of scattering blocking light to the detector.

Under acidic conditions, type-I collagen is highly soluble in a triple-helical form. In contrast to the case at pH 7, fibrillogenesis does not occur at higher temperatures in acidic conditions. Consistent with this, no change in G′ upon heating was observed for Telo-EPC in a 0.02 M AcA (pH 4) solution (Fig. 1 *A*). In CD, a single transition in MRE was observed at 42°C, associated with unfolding of soluble triple helices. The negative MRE transition only manifests under solution conditions in which collagen fibrillogenesis can occur.

Bovine type-I collagen from a different vendor (Telo-ABM, Advanced BioMatrix) and collagen from another species (rat) also showed the emergence of a large negative

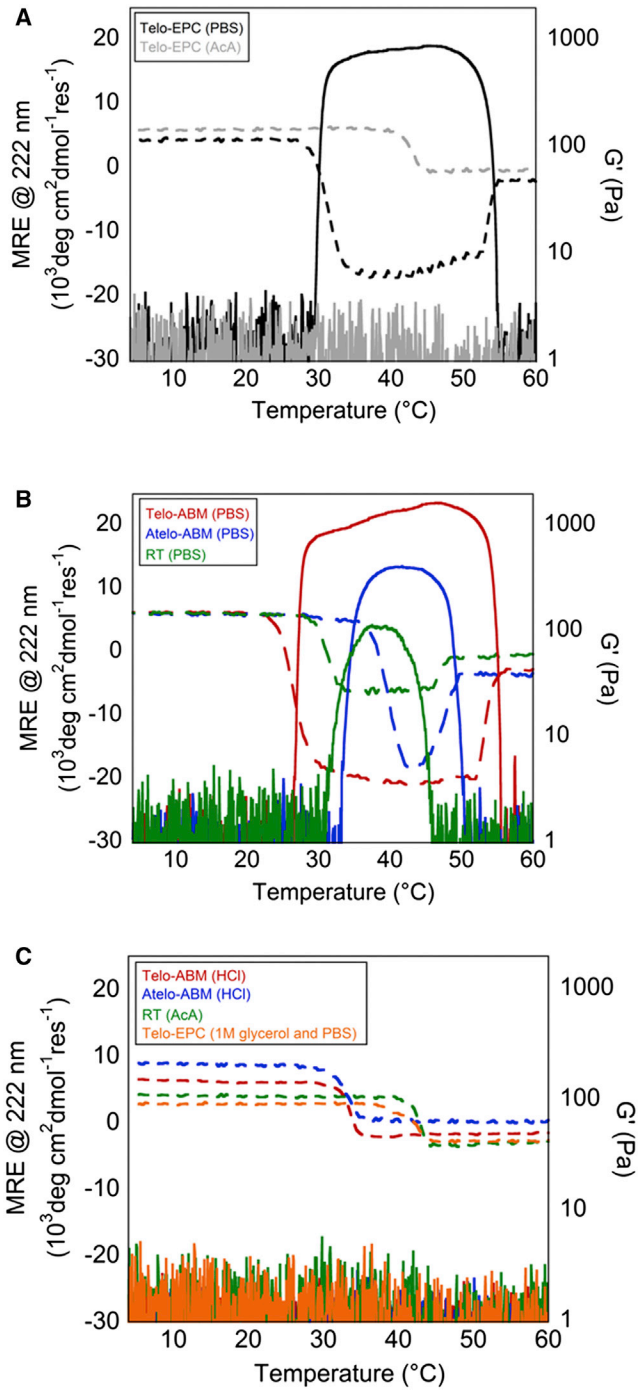

FIGURE 1 (*A*) MRE at 222 nm (*dashed lines*) and the storage modulus (G′) (*solid lines*) were measured from 4°C to 60°C for Telo-EPC in AcA versus neutral PBS buffers. Changes in MRE coincide with G′ upon fibrillogenesis and denaturation in neutral conditions. (*B*) A similar coincidence of MRE and G′ was observed for additional type-I collagen variants capable of self-assembly. (*C*) Telo-ABM, Atelo-ABM, and RT collagen in acidic conditions, and Telo-EPC in 1 M glycerol and PBS were incapable of self-assembly via rheology, and demonstrated only one transition from triple helix to a denatured state. To see this figure in color, go online.

MRE coincident with fibrillogenesis as observed by rheology (Fig. 1 *B*). This makes it highly unlikely that the negative band is due to contamination resulting from a particular extraction protocol or animal source. Pepsin digestion of collagen selectively removes portions of the C-terminal telopeptide, resulting in atelocollagen (Atelo-ABM), which alters fibrillogenesis behavior by raising the temperature at which fibrillogenesis occurs and lowering the temperature of denaturation. Despite these changes, fibrillogenesis was observed by both rheology and CD. Under acidic conditions, none of the collagen samples (Telo-ABM, Atelo-ABM, and RT) showed evidence of fibrillogenesis by either CD or rheology (Fig. 1 *C*). Glycerol also inhibits type-I collagen fibrillogenesis (37). Adding glycerol to Telo-EPC at neutral pH prevented fibrillogenesis as assessed by CD and rheology. Thus, a pronounced negative MRE transition was only observed for collagen preparations and solution conditions that facilitated fibrillogenesis.

CD signal unique to type-I collagen

Like type-I, type-III collagen is part of the fibril-forming family of collagens (11). Type-III collagen is frequently found on the periphery of type-I fibers in the skin and elsewhere (47). To determine whether a negative MRE signal is specifically diagnostic of interactions in type-I collagen fibrils, we monitored the MRE of type-III collagen in acidic and physiological buffers upon heating from 4°C to 60°C. Type-III, like type-I, was triple-helical at 4°C (Fig. S2). No negative MRE transition was observed when type-III collagen was heated under neutral or acidic solution conditions (Fig. 2). The concentration of type-III collagen necessary for rheological comparison was prohibitive, so self-assembly measurements were performed via light scattering (24). The derived count rate of

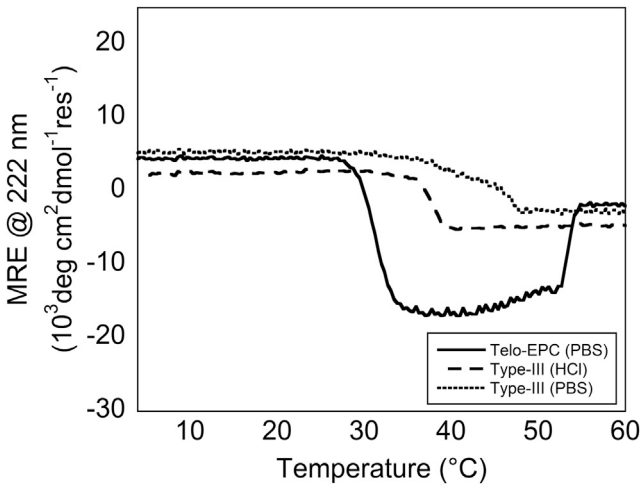

FIGURE 2 MRE at 222 nm of type-I and type-III collagen was measured from 4°C to 60°C. Telo-EPC samples in physiological buffer exhibited the two ellipticity transitions described in Fig. 1 *A*. Type-III samples in both acidic and physiological buffers exhibited one transition during heating.

type-III samples at neutral pH was below that of type-I (Fig. S4). Because type-III can rarely be isolated from type-I, self-assembly seen via light scattering may be the result of fibrillogenesis of either solely type-III or type-III collagen and contaminating type-I fibrils. Regardless, the emergence of the negative signal at 222 nm is not generalized to all fibril-forming members of collagen.

Gelatin does not show a characteristic CD signal

Collagen denaturation into gelatin is essentially irreversible, allowing us to determine whether the negative ellipticity is specific to the type-I collagen sequence or to specific interactions and structures as a result of ordered collagen fibrillogenesis. In contrast to the temperature-dependent behavior of type-I collagen, gelatin partially refolds into a triple helix and even forms networks at low temperatures (4°C), albeit at much higher concentrations (Fig. S5). Therefore, forward and reverse melts were performed on type-I collagen and gelatin to allow for self-assembly under both conditions, if possible. The two MRE transitions for Telo-EPC were seen in the forward melt, but were not apparent in the reverse melt (Fig. 3). Gelatin did not exhibit any significant negative MRE transition, indicating that the signal observed for type-I collagen may be specific to an ordered fibril composed of triple-helical units.

Monitoring fibrillogenesis at low concentrations

CD spectroscopy typically provides highly sensitive measurements, allowing the use of low sample volumes and concentrations. Telo-EPC solutions at concentrations of 0.01–0.1 mg/mL were monitored for fibrillogenesis via CD spectroscopy. At 4°C, the triple helix-positive MRE band at 222 nm was observed for collagen samples at concentrations of 0.05 mg/mL and 0.1 mg/mL (Fig. 4 *A*), but was not detected at lower concentrations. At 37°C, the magnitude of the negative MRE transition was significantly larger, and was clearly observed for all but the lowest concentration (Fig. 4 *B*). Upon further heating, the signal for samples above concentrations of 0.01 mg/ml returned to a level consistent with thermal denaturation. The critical temperature for fibrillogenesis increased with decreasing concentrations, consistent with previous observations (48).

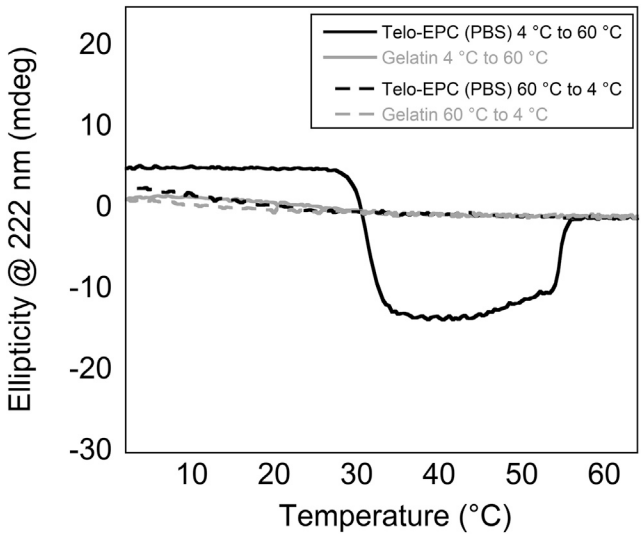

FIGURE 3 The ellipticity at 222 nm of Telo-EPC and gelatin samples was examined from 4°C to 60°C (forward melt, *solid lines*) and back to 4°C (reverse melt, *dashed lines*). Telo-EPC exhibited two transitions in MRE during the forward melt, and the triple-helical signal returned at low temperatures. The gelatin further denatured during heating and slightly refolded during cooling.

Identifying the fibril CD spectrum

Experiments primarily monitored ellipticity changes at 222 nm, as changes in the positive band at this wavelength are sensitive to triple helix structure. However, the collagen fibril potentially has a distinct spectral signature. Accordingly, a series of spectra from 200 to 260 nm were captured from 4°C to 60°C in 1°C increments. As the temperature increased, significant changes occurred in the spectral shape between the triple helix spectra at low temperatures and the random coil spectra at high temperatures (Fig. 5 *A*). At fibrillogenesis temperatures, the spectra lacked the positive band at 222 nm and had a pronounced negative band around 204–210 nm. These spectra could not be reconstructed by a superposition of triple-helical and denatured spectra, indicating the presence of other species. Two major transitions were observed in the spectra as a function of temperature: one near 30°C, coinciding with fibrillogenesis, and the other around 50°C, coinciding with denaturation (Fig. 5 *B*).

The CD signal at a given temperature is presumably a mixture of spectral components corresponding to triple helix, random coil, and one or several other species. The signal-processing algorithm fastICA was employed to reconstruct the observed spectra as a linear combination of such components. It was determined that three components were sufficient to reconstruct spectra from 4°C to 60°C (Fig. 6 *A*). If the components determined by fastICA were unconstrained, the spectral shapes did not correspond to those of known species such as the canonical triple helix and random coil. Therefore, we chose to constrain two of the three components to obtain triple helix and random coil shapes, respectively, and solved for the third component, the expected fibril spectrum. This analysis revealed that the fibril spectrum had a strong negative band around 204–210 nm—a new, to our knowledge, shape that does not match known secondary-structure spectra (Fig. 6 *B*). The emergence of this component coincident with fibrillogenesis was responsible for the observed change in ellipticity at 222 nm in the previous experiments.

It is possible to track the relative abundance of helix, fibril, and coil species with increasing temperature. The

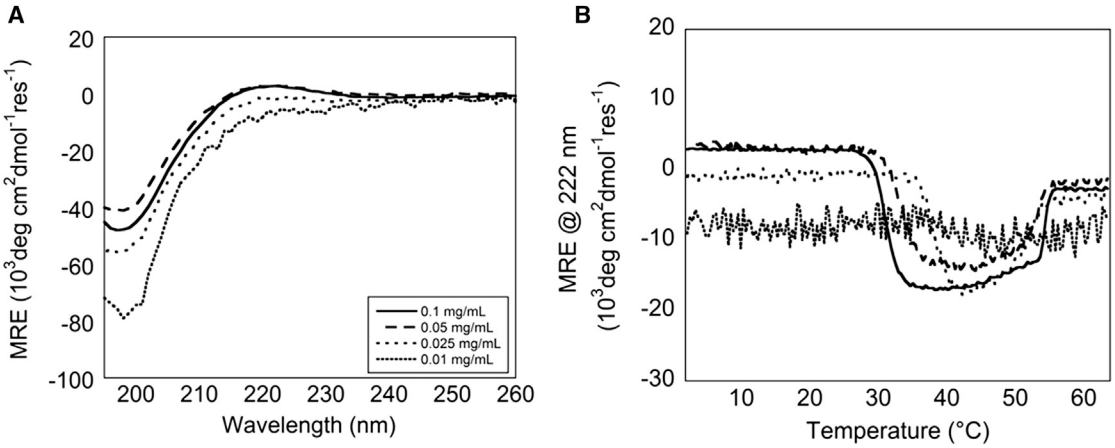

FIGURE 4 (*A*) Wavelength spectra were captured from Telo-EPC samples of decreasing concentrations at 4°C. (*B*) Sample MRE at 222 nm, monitored as a function of temperature. All concentrations above 0.01 mg/mL exhibited a measurable signal at 222 nm during fibrillogenesis.

weights of the three components required to reconstruct the experimental spectra as a function of temperature were extracted from the fastICA analysis (Fig. 6 *C*). Fitting fractional populations to a set of Hill-type parameters provided insight into the nature of the structural transitions from triple helix to fibril, and from fibril to denatured collagen (random coil) (Fig. S6). The first transition was characterized by a change from triple helix to fibril components at 25°C. This transition occurred over a short temperature range, consistent with the rapid fibril assembly upon nucleation observed by other methods. The loss of the fibril component and emergence of the denatured coil component coincided at ~45°C.

Monitoring collagen proteolysis in the fibril state

The ability to discriminate helix, fibril, and coil populations in a single sample can facilitate real-time observations of structural changes in collagen during biological processes. In the process of collagen degradation, bacterial collagenases cleave collagen relatively nonspecifically, whereas matrix metalloproteases often target a specific site on collagen (49). Given the challenges associated with monitoring the multiple structural forms of collagen simultaneously, little is known about how collagenase degradation proceeds. AFM imaging under solution conditions has provided some insight into real-time structural changes that occur during degradation (50). The ability to monitor the fibril state of collagen by CD should provide dynamic information about this process.

We monitored the enzymatic digestion of type-I collagen fibrils using the transition of the collagen fibril signal to random coil. Type-I collagenase recognizes and cleaves between the Y-Gly bonds in the …Gly-X-Y-Gly-X-Y… sequence (51). Collagen samples were measured for triple-helical signal at 4°C and then for fibril signal after 30 min incubation at 37°C before type-I collagenase was added to one of the samples (Fig. 7 *A*). Both samples were triple-helical at 4°C and formed fibrils, as assessed by CD at 37°C. When type-I collagen was treated with type-I collagenase, a lag phase of ~30 min was observed in the enzymatic activity, followed by a slow increase in the negative peak at 204 nm (Fig. 7 *B*). The signal transitioned to random coil quite rapidly after ~3 h (Fig. 7 *C*). The collagenase signal remained after digestion (Fig. S7).

Fitting of the obtained CD spectra to helix, fibril, and coil components suggested that digestion proceeds from a helix-fibril mixture to triple helix to coil (Fig. 7 *D*). The experimental and reconstructed spectra support AFM measurements that showed slow thinning of fibrils over time

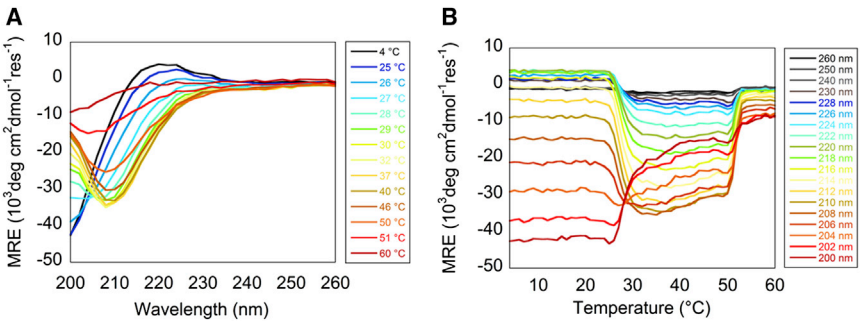

FIGURE 5 MRE as a function of wavelength and temperature was captured to monitor self-assembly and denaturation for a Telo-EPC sample. (*A*) Wavelength spectra were measured every degree from 4°C to 60°C. For clarity, only spectra where changes took place are shown. The collagen triple helix signal was clearly observed at 4°C as a positive peak at 222 nm and negative peak below 200 nm. The collagen fibril signal was observed as a negative peak at 210 nm. (*B*) The same spectra decomposed by wavelength and plotted against temperature. To see this figure in color, go online.

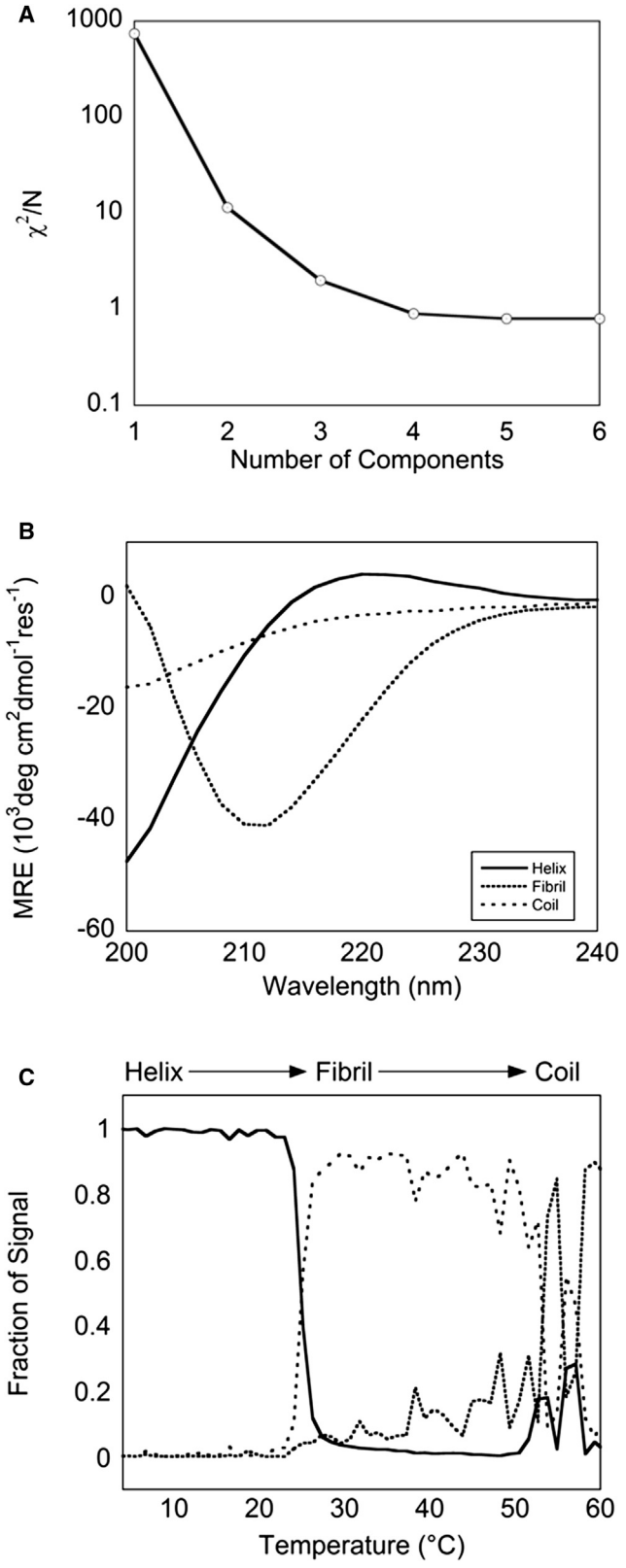

FIGURE 6 (*A*) In identifying a fibril spectral component in the temperature-dependent fibrillogenesis of Telo-EPC, analysis indicated that three components were sufficient to recover experimental spectra at all temperatures ($\chi^2/N = 2.0$ for $N = 3$). (*B*) In addition to constrained helix and coil components, a fibril spectral component was identified with a negative band at 210 nm for this experiment. (*C*) The fraction of signal of the three species as a function of temperature reveals two transitions—from helix to fibril, and from fibril to coil—as previously identified in the Telo-EPC temperature melt data (Fig. 1 *A*).

(50). Combining CD with other structure-characterization methods on similarly prepared samples will provide insights into collagen remodeling processes such as this at multiple levels of structural detail.

DISCUSSION

There is strong evidence that assembled collagen fibrils contribute a unique CD spectral component. This collagen fibril spectrum is distinct from a soluble triple helix and is similar in spectral shape to the polyproline II structure but has a much larger magnitude (Fig. S8) (52,53). This signal is strongly correlated with other measurements of fibrillogenesis, such as rheology and light scattering, and is evident for a number of type-I collagens from diverse source tissues and species. Solution conditions that inhibit fibril formation prevent this spectral component from being observed, indicating that a contaminating signal from another protein is unlikely.

CD spectroscopy experiments were performed at much slower heating and cooling rates in comparison with rheology. In rheology, faster temperature rates were required to confidently avoid sample dehydration. Despite these differences in experimental conditions and collagen concentrations, the emergence of a negative signal occurred at approximately the same temperature as fibrillogenesis. Rheology and CD spectroscopy captured differences in the kinetics of self-assembly: when telo- and atelocollagens were compared, the presence of the telopeptides appeared to catalyze fibril formation, which is a well-characterized phenomenon in the literature (54–56). Additionally, rheology and CD demonstrated that the transition to gelatin occurred at lower temperatures for RT collagen than for bovine skin collagen, implying a difference in fibril stability between species of type-I collagen. The unique temperature-dependent profiles of the negative MRE signal suggest that the collagen fibril spectrum provides information about the kinetics of fibrillogenesis and potentially speaks to the structural changes that occur as a result of fibril formation.

The molecular structure that causes this spectroscopic signal appears to be specific to type-I collagen fibrillogenesis. Other forms of aggregation, such as amyloid aggregation, occur after protein unfolding and result in a large increase in dynode voltage due to scattering (57), which was not observed in our measurements (Fig. S3). When the evolution of this signal was captured as a function of temperature, it was clear that the emergence of a strong negative signal in regions between 204 and 210 nm was the dominant signal change at temperatures for self-assembly, decreasing

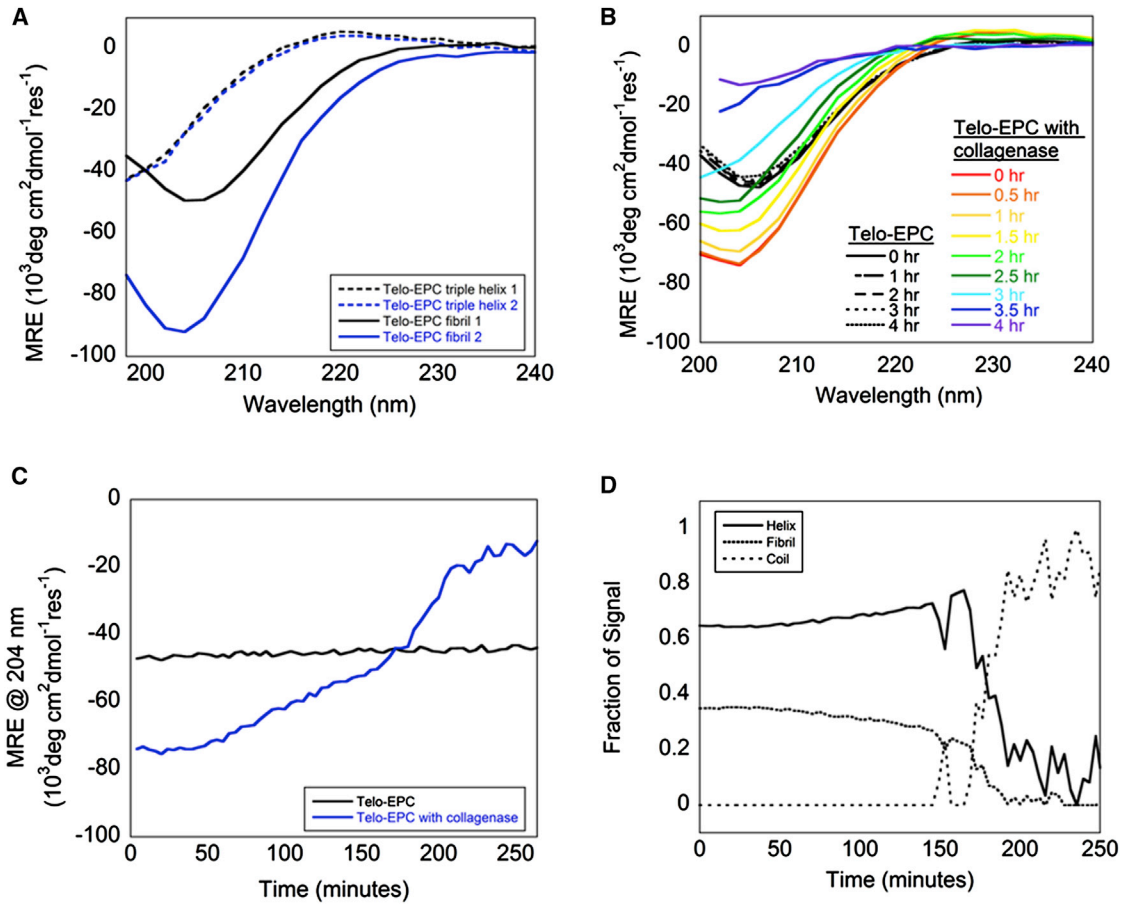

FIGURE 7 (*A*) Telo-EPC samples were measured for triple-helical content and fibril content as the ellipticity was measured from 198 to 240 nm. Samples 1 and 2 were prepared identically, but sample 2 was ultimately treated with collagenase. (*B*) A series of wavelength spectra were obtained over a period of 4 h after collagenase addition. Data obtained at later times after the dynode voltage exceeded 600 V were not included in the analysis. The collagen sample with added collagenase was digested over the course of 4 h as measured by the increase in signal at 204 nm. (*C*) Sample MRE at 204 nm, plotted as a function of time. (*D*) Previously identified components were fit to the collagenase data and demonstrated substantial helix (~62%) and fibril (~38%) components before degradation occurred. To see this figure in color, go online.

the MRE at 222 nm. Given the magnitude of this effect, we are likely observing structural changes that affect a significant fraction of backbone peptide bonds, resulting in unique excitonic couplings upon fibril formation.

Although the exact structural and photophysical origins of the collagen fibril spectrum remain to be determined, this signature is useful for studying collagen fibrillogenesis and measures of fibril stability. Measurements reported to date indicate that this signal appears as early as 10 min after incubation at 37°C (24) and is stable for a minimum of 12 h (Fig. S9). This is particularly advantageous for studies of mutated collagens and/or collagen mimetic peptides, when sample availability is problematic. Together with CD spectroscopy, this unique spectroscopic signal may provide further insights into the process of collagen fibrillogenesis and/or the specific molecular interactions that promote or inhibit fibril formation.

CD spectroscopy may also be useful in materials science research to understand structural changes associated with collagen modifications through chemical or UV cross-linking or molecular coupling of chemical moieties. Herein, we have demonstrated how CD spectroscopy can be expanded to estimate the secondary structure of type-I collagen monomers and fibrils, and to follow the evolution of the collagen fibril signal, which will facilitate medical research involving collagen structure and fibrillogenesis.

SUPPORTING MATERIAL

Supporting Materials and Methods, nine figures, one table, and one data file are available at http://www.biophysj.org/biophysj/supplemental/S0006-3495(16)30950-X.

AUTHOR CONTRIBUTIONS

K.E.D. designed and performed research, analyzed data, and wrote the manuscript. D.R.G. designed and performed research, and analyzed data. A.S.P. designed research and analyzed data. V.N. designed and performed research, contributed analytic tools, analyzed data, and wrote the manuscript. D.I.S. designed research, contributed analytic tools, and wrote the manuscript. All authors approved the final version of the manuscript.

ACKNOWLEDGMENTS

This project was supported in part by the National Science Foundation (grants ARRA-CBET0846328 and DMR-0907273); the Office of the Director, National Institutes of Health (DP2-OD-006478-1), the Department of Science and Technology, India (SB/FTP/PS-073/2014), fellowships from the National Science Foundation (NSF DGE 0801620, IGERT: Integrated Science and Engineering of Stem Cells), Rutgers Biotechnology Training Program (National Institutes of Health grant 5T32GM008339-20), Department of Education Graduate Assistance in Areas of National Need, and a Scholar Award given by the International Chapter of the P.E.O. Sisterhood.

We dedicate this study to Jack Aviv in memory of his commitment to and support of the biophysical community.

SUPPORTING CITATIONS

References (58–60) appear in the Supporting Material.

REFERENCES

1. Abou Neel, E. A., L. Bozec, …, J. K. Hyun. 2013. Collagen—emerging collagen based therapies hit the patient. *Adv. Drug Deliv. Rev.* 65:429–456.
2. Glowacki, J., and S. Mizuno. 2008. Collagen scaffolds for tissue engineering. *Biopolymers.* 89:338–344.
3. Chevallay, B., and D. Herbage. 2000. Collagen-based biomaterials as 3D scaffold for cell cultures: applications for tissue engineering and gene therapy. *Med. Biol. Eng. Comput.* 38:211–218.
4. Parenteau-Bareil, R., R. Gauvin, and F. Berthod. 2010. Collagen-based biomaterials for tissue engineering applications. *Materials (Basel).* 3:1863–1887.
5. Engler, A. J., S. Sen, …, D. E. Discher. 2006. Matrix elasticity directs stem cell lineage specification. *Cell.* 126:677–689.
6. Dantzer, E., P. Queruel, …, J. F. Quinot. 2003. Dermal regeneration template for deep hand burns: clinical utility for both early grafting and reconstructive surgery. *Br. J. Plast. Surg.* 56:764–774.
7. Clayman, M. A., S. M. Clayman, and D. W. Mozingo. 2006. The use of collagen-glycosaminoglycan copolymer (Integra) for the repair of hypertrophic scars and keloids. *J. Burn Care Res.* 27:404–409.
8. Helfrich, Y. R., D. L. Sachs, and J. J. Voorhees. 2008. Overview of skin aging and photoaging. *Dermatol. Nurs.* 20:177–183, quiz 184.
9. Prockop, D. J., K. I. Kivirikko, …, N. A. Guzman. 1979. The biosynthesis of collagen and its disorders (first of two parts). *N. Engl. J. Med.* 301:13–23.
10. Prockop, D. J., K. I. Kivirikko, …, N. A. Guzman. 1979. The biosynthesis of collagen and its disorders (second of two parts). *N. Engl. J. Med.* 301:77–85.
11. Ricard-Blum, S. 2011. The collagen family. *Cold Spring Harb. Perspect. Biol.* 3:a004978.
12. Orgel, J. P., J. D. San Antonio, and O. Antipova. 2011. Molecular and structural mapping of collagen fibril interactions. *Connect. Tissue Res.* 52:2–17.
13. Muiznieks, L. D., and F. W. Keeley. 2013. Molecular assembly and mechanical properties of the extracellular matrix: A fibrous protein perspective. *Biochim. Biophys. Acta.* 1832:866–875.
14. Kadler, K. E., D. F. Holmes, …, J. A. Chapman. 1996. Collagen fibril formation. *Biochem. J.* 316:1–11.
15. Green, H., and B. Goldberg. 1964. Collagen and cell protein synthesis by an established mammalian fibroblast line. *Nature.* 204:347–349.
16. Green, H., B. Goldberg, and G. J. Todaro. 1966. Differentiated cell types and the regulation of collagen synthesis. *Nature.* 212:631–633.
17. Harris, J. R., A. Soliakov, and R. J. Lewis. 2013. In vitro fibrillogenesis of collagen type I in varying ionic and pH conditions. *Micron.* 49:60–68.
18. Christiansen, D. L., E. K. Huang, and F. H. Silver. 2000. Assembly of type I collagen: fusion of fibril subunits and the influence of fibril diameter on mechanical properties. *Matrix Biol.* 19:409–420.
19. Hyashi, T., S. Curran-Patel, and D. J. Prockop. 1979. Thermal stability of the triple helix of type I procollagen and collagen. Precautions for minimizing ultraviolet damage to proteins during circular dichroism studies. *Biochemistry.* 18:4182–4187.
20. Li, Y., and E. P. Douglas. 2013. Effects of various salts on structural polymorphism of reconstituted type I collagen fibrils. *Colloids Surf. B Biointerfaces.* 112:42–50.
21. Nikolaeva, T. I., S. M. Kuznetsova, and V. V. Rogachevsky. 2013. [Collagen fibril formation in vitro at nearly physiological temperatures]. *Biophysics (Oxf.).* 57:757–763.
22. Kadler, K. E., Y. Hojima, and D. J. Prockop. 1988. Assembly of type I collagen fibrils de novo. Between 37 and 41 degrees C the process is limited by micro-unfolding of monomers. *J. Biol. Chem.* 263:10517–10523.
23. Li, J., and G. Li. 2011. The thermal behavior of collagen in solution: effect of glycerol and 2-propanol. *Int. J. Biol. Macromol.* 48:364–368.
24. Drzewiecki, K. E., A. S. Parmar, …, D. I. Shreiber. 2014. Methacrylation induces rapid, temperature-dependent, reversible self-assembly of type-I collagen. *Langmuir.* 30:11204–11211.
25. Brodsky, B., and J. A. M. Ramshaw. 1997. The collagen triple-helix structure. *Matrix Biol.* 15:545–554.
26. Greenfield, N. J. 2006. Using circular dichroism spectra to estimate protein secondary structure. *Nat. Protoc.* 1:2876–2890.
27. Silver, F. H., and D. E. Birk. 1983. Kinetic analysis of collagen fibrillogenesis: I. Use of turbidity-time data. *Coll. Relat. Res.* 3:393–405.
28. Li, Y., A. Asadi, …, E. P. Douglas. 2009. pH effects on collagen fibrillogenesis in vitro: electrostatic interactions and phosphate binding. *Mater. Sci. Eng. C.* 29:1643–1649.
29. Williams, B. R., R. A. Gelman, …, K. A. Piez. 1978. Collagen fibril formation. Optimal in vitro conditions and preliminary kinetic results. *J. Biol. Chem.* 253:6578–6585.
30. Stoller, P., P. M. Celliers, …, A. M. Rubenchik. 2003. Quantitative second-harmonic generation microscopy in collagen. *Appl. Opt.* 42:5209–5219.
31. Theodossiou, T. A., C. Thrasivoulou, …, D. L. Becker. 2006. Second harmonic generation confocal microscopy of collagen type I from rat tendon cryosections. *Biophys. J.* 91:4665–4677.
32. Chen, X., O. Nadiarynkh, …, P. J. Campagnola. 2012. Second harmonic generation microscopy for quantitative analysis of collagen fibrillar structure. *Nat. Protoc.* 7:654–669.
33. Boldon, L., F. Laliberte, and L. Liu. 2015. Review of the fundamental theories behind small angle X-ray scattering, molecular dynamics simulations, and relevant integrated application. *Nano Rev.* 6:25661.
34. Bentz, H., H. P. Bächinger, …, K. Kühn. 1978. Physical evidence for the assembly of A and B chains of human placental collagen in a single triple helix. *Eur. J. Biochem.* 92:563–567.
35. Gayatri, R., A. K. Sharma, …, T. Ramasami. 2001. Chromium(III)-induced structural changes and self-assembly of collagen. *Biochem. Biophys. Res. Commun.* 283:229–235.
36. Ikoma, T., H. Kobayashi, …, S. Mann. 2003. Physical properties of type I collagen extracted from fish scales of Pagrus major and Oreochromis niloticas. *Int. J. Biol. Macromol.* 32:199–204.
37. Leikina, E., M. V. Mertts, …, S. Leikin. 2002. Type I collagen is thermally unstable at body temperature. *Proc. Natl. Acad. Sci. USA.* 99:1314–1318.
38. Madhan, B., V. Subramanian, …, T. Ramasami. 2005. Stabilization of collagen using plant polyphenol: role of catechin. *Int. J. Biol. Macromol.* 37:47–53.
39. Peltonen, L., A. Palotie, …, D. J. Prockop. 1980. Thermal stability of type I and type III procollagens from normal human fibroblasts and from a patient with osteogenesis imperfecta. *Proc. Natl. Acad. Sci. USA.* 77:162–166.

40. Schmid, T. M., and T. F. Linsenmayer. 1984. Denaturation-renaturation properties of two molecular forms of short-chain cartilage collagen. *Biochemistry.* 23:553–558.

41. Scott, P. G. 1986. Spectroscopic study of environment-dependent changes in the conformation of the isolated carboxy-terminal telopeptide of type I collagen. *Biochemistry.* 25:974–980.

42. Zhang, Z., G. Li, and B. Shi. 2005. Physicochemical properties of collagen, gelatin and collagen hydrolysate derived from bovine limed split washes. *J. Soc. Leather Technol.Chemists.* 90:23–28.

43. Persikov, A. V., Y. Xu, and B. Brodsky. 2004. Equilibrium thermal transitions of collagen model peptides. *Protein Sci.* 13:893–902.

44. Hennessey, J. P., Jr., and W. C. Johnson, Jr. 1981. Information content in the circular dichroism of proteins. *Biochemistry.* 20:1085–1094.

45. Hyvärinen, A., and E. Oja. 2000. Independent component analysis: algorithms and applications. *Neural Netw.* 13:411–430.

46. Hyvärinen, A. 1999. Fast and robust fixed-point algorithms for independent component analysis. *IEEE Trans. Neural Netw.* 10:626–634.

47. Fleischmajer, R., E. D. MacDonald, …, L. W. Fisher. 1990. Dermal collagen fibrils are hybrids of type I and type III collagen molecules. *J. Struct. Biol.* 105:162–169.

48. Wood, G. C., and M. K. Keech. 1960. The formation of fibrils from collagen solutions. 1. The effect of experimental conditions: kinetic and electron-microscope studies. *Biochem. J.* 75:588–598.

49. Birkedal-Hansen, H., W. G. I. Moore, …, J. A. Engler. 1993. Matrix metalloproteinases: a review. *Crit. Rev. Oral Biol. Med.* 4:197–250.

50. Paige, M., A. Lin, and C. Goh. 2002. Real-time enzymatic biodegradation of collagen fibrils monitored by atomic force microscopy. *Int. Biodeterior. Biodegradation.* 20:1–10.

51. Barrett, A. J., N. D. Rawlings, and J. F. Woessner. 1998. Handbook of Proteolytic Enzymes. Elsevier Academic Press, London.

52. Lopes, J. L., A. J. Miles, L. Whitmore, and B. A. Wallace. 2014. Distinct circular dichroism spectroscopic signatures of polyproline II and unordered secondary structures: applications in secondary structure analyses. *Protein Sci.* 23:1765–1772.

53. Wallace, B., and R. Janes. 2016. Protein Circular Dichroism Data Bank. Department of Crystallography, Institute of Structural and Molecular Biology, Birkbeck College, University of London, School of Biological and Chemical Sciences, Queen Mary, University of London, UK.

54. Kuznetsova, N., and S. Leikin. 1999. Does the triple helical domain of type I collagen encode molecular recognition and fiber assembly while telopeptides serve as catalytic domains? Effect of proteolytic cleavage on fibrillogenesis and on collagen-collagen interaction in fibers. *J. Biol. Chem.* 274:36083–36088.

55. Comper, W. D., and A. Veis. 1977. The mechanism of nucleation for in vitro collagen fibril formation. *Biopolymers.* 16:2113–2131.

56. Helseth, D. L., Jr., and A. Veis. 1981. Collagen self-assembly in vitro. Differentiating specific telopeptide-dependent interactions using selective enzyme modification and the addition of free amino telopeptide. *J. Biol. Chem.* 256:7118–7128.

57. Benjwal, S., S. Verma, K. H. Rohm, and O. Gursky. 2006. Monitoring protein aggregation during thermal unfolding in circular dichroism experiments. *Protein Sci.* 15:635–639.

58. Whitmore, L., and B. A. Wallace. 2008. Protein secondary structure analyses from circular dichroism spectroscopy: methods and reference databases. *Biopolymers.* 89:392–400.

59. Whitmore, L., and B. A. Wallace. 2004. DICHROWEB, an online server for protein secondary structure analyses from circular dichroism spectroscopic data. *Nucleic Acids Res.* 32:W668–W673.

60. Lobley, A., L. Whitmore, and B. A. Wallace. 2002. DICHROWEB: an interactive website for the analysis of protein secondary structure from circular dichroism spectra. *Bioinformatics.* 18:211–212.

Biophysical Journal, Volume *111*

Supplemental Information

Circular Dichroism Spectroscopy of Collagen Fibrillogenesis: A New Use for an Old Technique

Kathryn E. Drzewiecki, Daniel R. Grisham, Avanish S. Parmar, Vikas Nanda, and David I. Shreiber

Supporting Methods

Transmission Electron Microscopy

Type-I collagen samples (Telo-EPC) were prepared and imaged as described previously (1). In brief, collagen suspensions were prepared as described in the Rheology section of the Methods in the main text and incubated for 30 minutes at 37 °C in microfuge tubes. A 10 μL sample of the supernatant of the gel was plated on a plastic Petri dish, and an extra-thick carbon mesh copper grid was placed on the droplet for 5 minutes. The supernatant was removed using filter paper, and then the grid was stained with 1% phosphotungstic acid for 5 minutes. Samples were dried overnight and imaged using a JEM-100CX TEM microscope.

Rheology

Type-I collagen samples (Telo-EPC) for rheological testing were prepared and loaded on the rheometer as described in the main text. The temperature was immediately raised to 37 °C, and the sample was continually oscillated to 0.5% strain at 1 rad/s for 10 minutes while measuring the resultant torque to obtain the temperature-dependent sample storage and loss moduli (G′ and G″, respectively).

Gelatin samples were assayed for hydrogel formation. Samples were prepared at 25 mg/mL in PBS, and were fully solubilized by heating to 37 °C. Rheology measurements were performed differently for gelatin compared to type-I collagen, which forms a hydrogel at low temperatures (~4 °C) rather than physiological temperature (37 °C). To perform these measurements, samples were plated at 25 °C, then the temperature was increased to 37 °C to ensure the gelatin was fully fluid, decreased to 4 °C at a rate of 2 °C/minute, and held at 4 °C for 15 minutes to assay for hydrogel formation. Measurements of three separately prepared samples were taken and averaged.

Light Scattering

Light scattering measurements were performed on a Zetasizer Nano ZS (Malvern Instruments, Malvern, UK) with a 3mW He-Ne laser at $\lambda = 633$ nm, collecting backscattered light at $\theta = 173°$. A built-in Peltier element controlled sample temperature during measurements to within ±0.1 °C. Scattering intensities and autocorrelation functions were determined from the average of either three or five correlation functions, with a typical acquisition time of 60 s per correlation function. Type-I (Telo-EPC) and type-III collagen solutions were prepared in PBS buffer (final concentration of 0.1 mg/mL). Samples were loaded into low-volume quartz batch cuvettes (ZEN2112) and equilibrated to 37 °C. Measurements of three separately prepared samples of each type were taken every minute for 30 minutes and averaged.

ICA Software

Source code for Independent Component Analysis is provided in the supporting file `itpp_ICA.zip`. It includes the it++ library (http://itpp.sourceforge.net) and supporting code for implementing ICA on CD data provided in the AVIV CD spectrometer output file format. Instructions for installation, required supporting libraries and usage are provided in `READ_ME.txt`. Code developed specifically for this project and it++ including modifications to the library are distributed under the pre-existing GNU General Public License (http://www.gnu.org/copyleft/gpl.html).

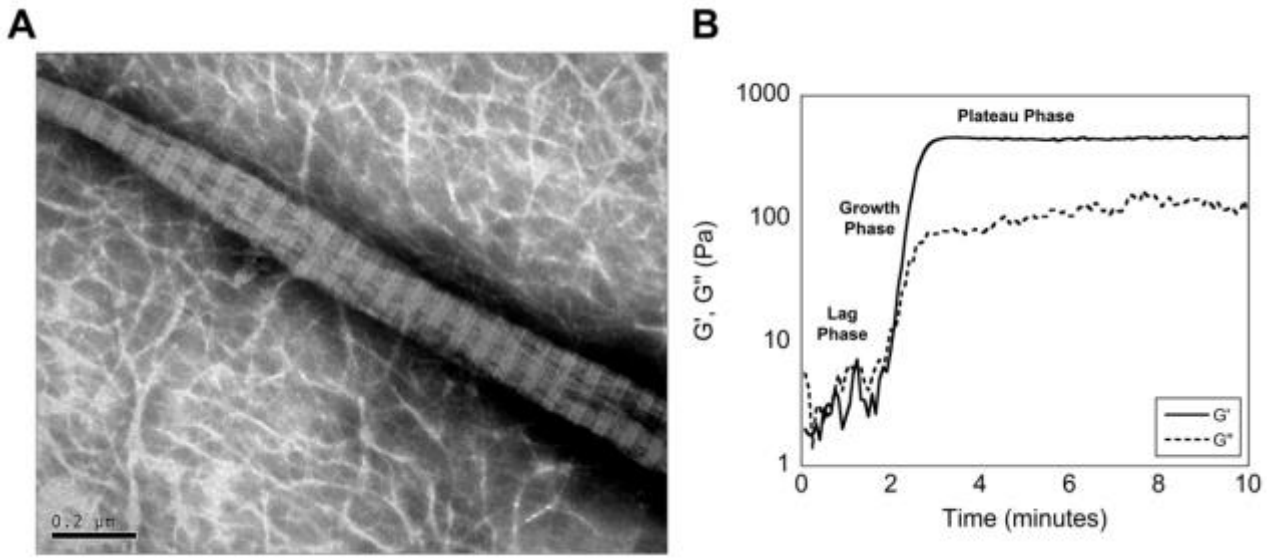

Figure S1. A) Ordered D-banding in collagen fibrils was visualized by Transmission Electron Microscopy. B) Rheology allows for characterization of the mechanical properties of type-I collagen hydrogels; the process of collagen fibrillogenesis manifests as a lag phase, where the storage modulus and loss modulus (G′ and G′′, respectively) are negligible, a growth phase of fibril formation, exhibited as an increase in both G′ and G′′, and a plateau phase indicative of fibril stabilization, where G′ and G′′ are constant.

Experiment Number	Samples	Wavelength (nm)	Temperature (°C)	Averaging Time (s)	Wavelength Increment (nm)	Temperature Step (°C)	Equilibration Time (min)	Notes
1	Telo-EPC, Telo-ABM, Atelo-ABM, RT, Type-III, Gelatin	260-195	4	10	1	N/A	2	• All samples at 0.1 mg/mL except Telo-EPC at 0.1, 0.05, 0.025, and 0.01 mg/mL
		222	4-60	10	N/A	0.33	2	• All samples at 0.1 mg/mL except Telo-EPC at 0.1, 0.05, 0.025, and 0.01 mg/mL • Performed from 4 °C to 60 °C and returned to 4 °C
2	Telo-EPC	260-200	4-60	3	2	0.33	6	• N/A
3	Telo-EPC with and without type-I collagenase	240-198	4	3	2	N/A	2	• Telo-EPC prepared at 0.05 mg/mL in PBS • Sample volumes of 250 µL
		240-198	37	3	2	N/A	2	• Samples from above given 1 hour for self-assembly
		240-200	37	3	2	N/A	2	• 50 µL of either 0.04 mM $CaCl_2$ (Fisher) in PBS (Fisher) or 3 mg/mL type-I collagenase (C1030, Sigma) in 0.04 mM $CaCl_2$ in PBS was added to each cuvette prior to measurement

Table S1. Parameters of CD Spectroscopy experiments for each set of collagen samples with additional notes to clarify procedures.

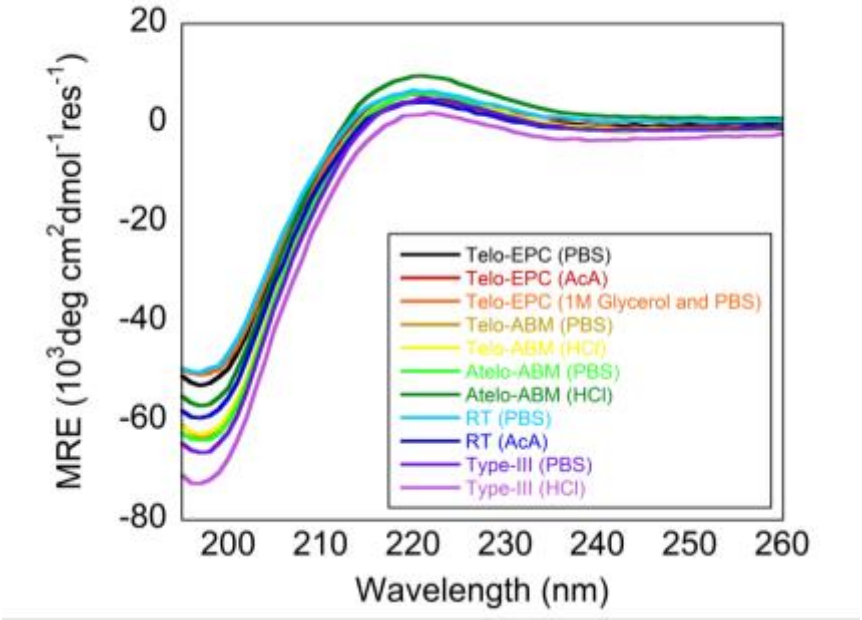

Figure S2. Mean residue ellipticity (MRE) of collagen samples was measured from 195 – 260 nm at 4 ºC. All collagens, regardless of buffer, demonstrated triple-helical content via CD measurements as a positive peak at 222 nm and a negative peak near 195 nm.

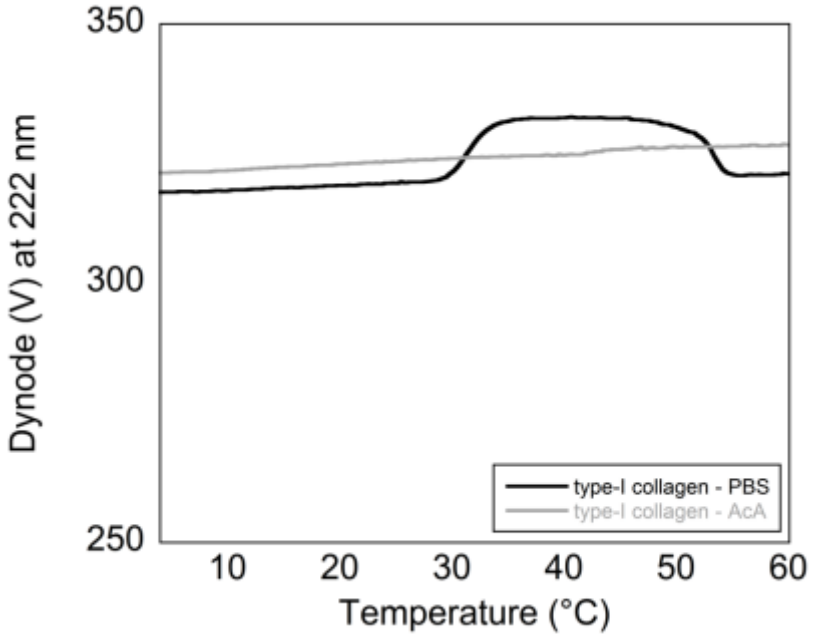

Figure S3. Representative example of the change in dynode voltage at 222 nm throughout a temperature melt experiment (Fig. 1 *A*) with type-I collagen (Telo-EPC) in acidic (AcA) and physiological (PBS) buffers. The dynode voltage did not exceed 600 V, which indicated that the change in ellipticity was due to structural changes in the protein sample and not the result of light scattering.

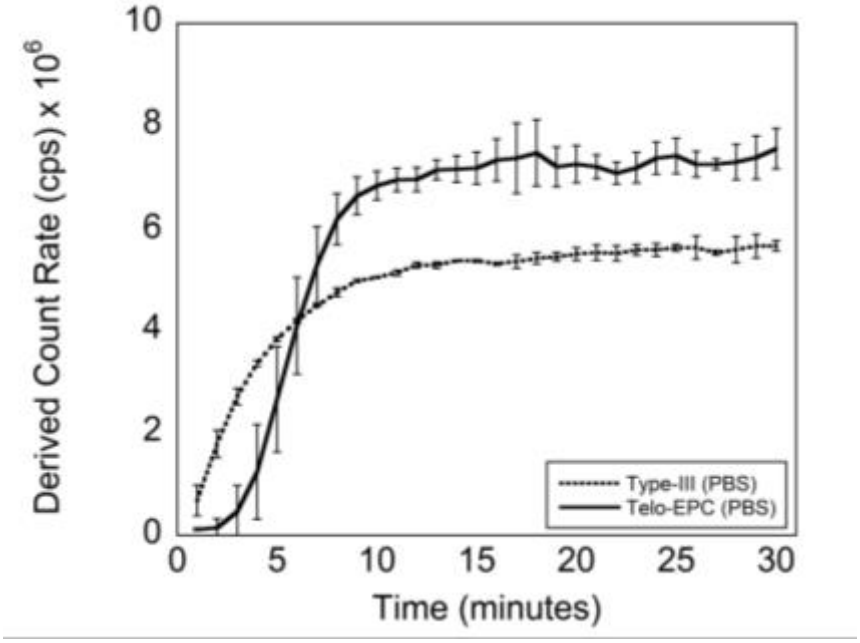

Figure S4. The derived count rate of type-I (Telo-EPC) and type-III collagen samples was monitored at 37 ºC as samples formed fibrils. Error bars represent the average measurement for three samples. Telo-EPC and type-III samples were both capable of self-assembly, demonstrated as an increase in derived count rate during heating presumably due to fibril formation. Type-I and type-III collagen are very difficult to isolate from one another, therefore, it is not possible to determine if the increase in scattering as seen in these results is due to fibrillogenesis of solely type-III or type-I and type-III fibrils.

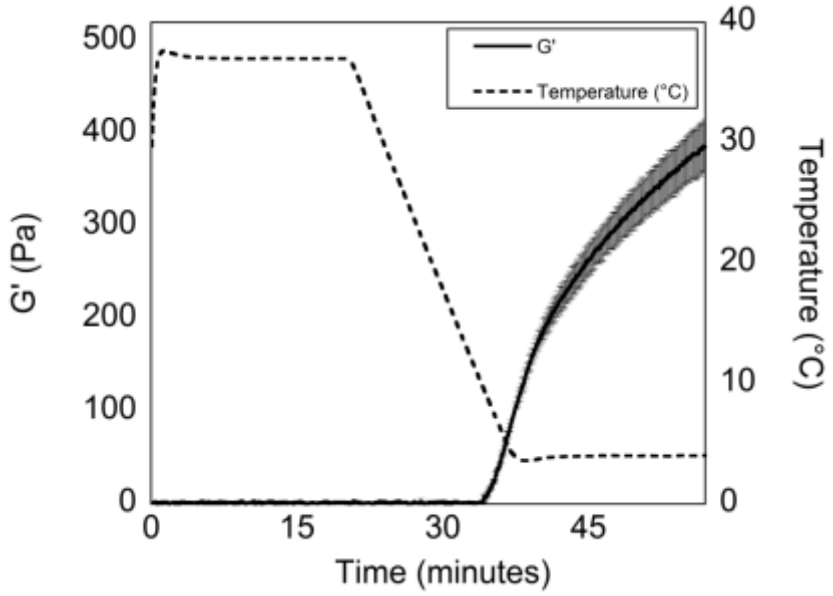

Figure S5. The increase in storage modulus at temperatures below 10 °C indicates that gelatin is capable of forming a hydrogel at relatively high concentrations and low temperatures. Error bars represent the average measurement of three samples.

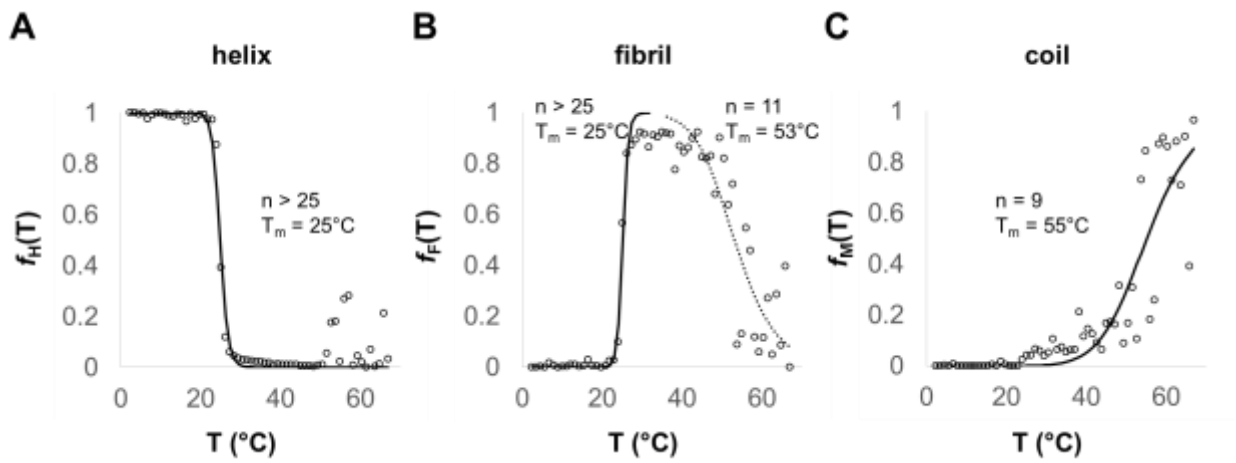

Figure S6. $f_H(T)$, $f_F(T)$ and $f_M(T)$ corresponding to fractional helix (A), fibril (B), and coil (C) species from deconvolution of the Telo-EPC melt (Fig. 5 and Fig. 6). Fractional populations were fit to a Hill-plot function: $f = T^n / (T^n + T_m^n)$, with n as the steepness of the transition at temperature T_m. Helix and coil (A and C) fractional populations were each fit to one transition. Fibril (B) fractional populations were fit to two transitions corresponding to the emergence (solid line) and loss (dotted line) of this species.

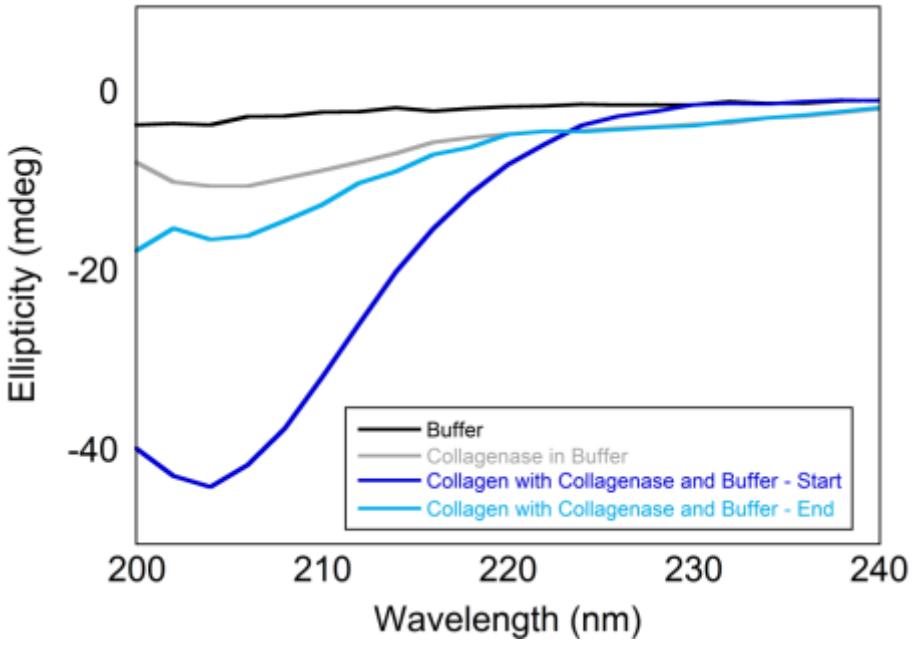

Figure S7. Raw wavelength spectra of buffer, type-I collagenase in buffer, and the starting and ending spectra of type-I collagen with collagenase from 200 – 240 nm. There are no buffer/enzyme subtraction or MRE correction in this figure. The collagenase signal was slightly more negative in the lower wavelength regions compared to the buffer signal. When collagen and collagenase were in the cuvette at the beginning of the measurement, the measurement was primarily our fibrillar collagen with the negative peak at ~204 nm. When the collagen was digested we saw a similar spectra compared to the original collagenase signal, presumably with some fragments of type-I collagen remaining.

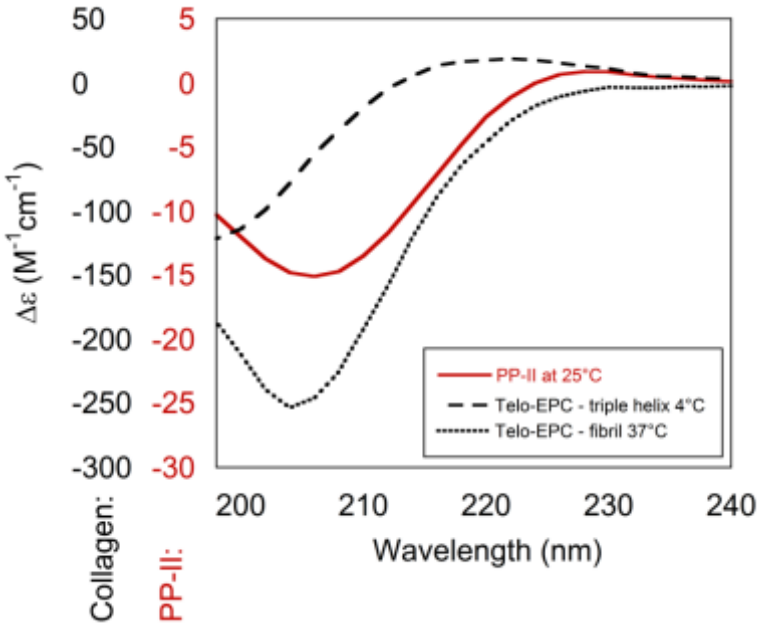

Figure S8. Wavelength spectra of Telo-EPC in triple-helical (4 °C) and fibril states (37 °C) (from Fig. 5 *A*) were compared to the poly-proline II (PP-II) signal obtained by Lopes et al (2). To ensure the units were the same, MRE of our collagen signals was converted to Δε (3-5). Note that the collagen signals are an order of magnitude greater than the PP-II signal. Signal information for PP-II was downloaded from the Protein Circular Dichroism Data Bank (6). The PP-II from Lopes et al (2) was purchased from Sigma-Aldrich, and had a molecular weight of 1,000 Da – 10,000 Da in comparison to the collagen triple-helix, which is ~350,000 Da. The Telo-EPC triple-helix signal and PP-II signal are clearly distinct, particularly when comparing the positive peak at 222 nm and the lack of a negative peak at 204 nm. The CD signature of Telo-EPC fibril signal and PP-II are similar in spectral shape, but the amplitude of the peaks differ by over an order of magnitude.

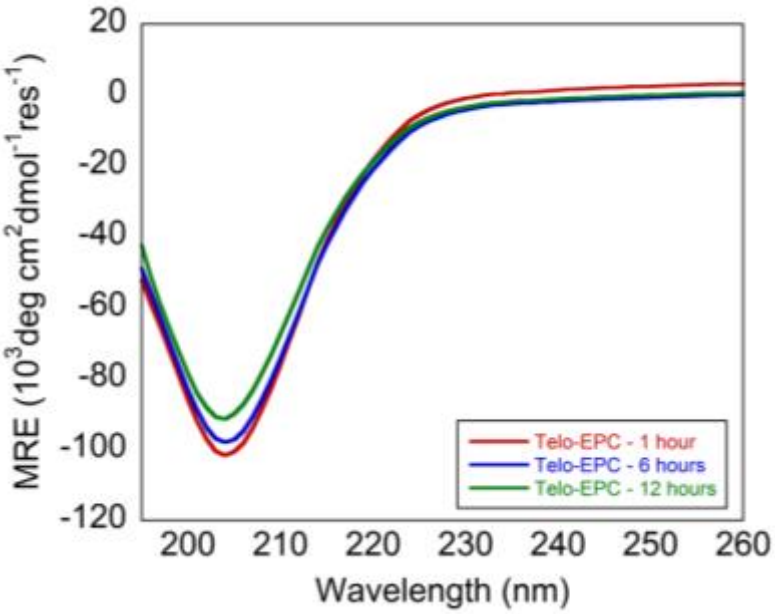

Figure S9. Wavelength spectra of Telo-EPC were measured every hour for 12 hours as outlined in Table S1, Experiment 1, but at 37 ℃. The negative peak at 210 nm was stable over the course of 12 hours.

Supporting References

1. Drzewiecki, K. E., A. S. Parmar, I. D. Gaudet, J. R. Branch, D. H. Pike, V. Nanda, and D. I. Shreiber. 2014. Methacrylation induces rapid, temperature-dependent, reversible self-assembly of type-I collagen. Langmuir : the ACS journal of surfaces and colloids 30:11204-11211.

2. Lopes, J. L., A. J. Miles, L. Whitmore, and B. A. Wallace. 2014. Distinct circular dichroism spectroscopic signatures of polyproline II and unordered secondary structures: applications in secondary structure analyses. Protein science : a publication of the Protein Society 23:1765-1772.

3. Whitmore, L. and B. A. Wallace. 2008. Protein Secondary Structure Analyses from Circular Dichroism Spectroscopy: Methods and Reference Databases. Biopolymers 89: 392-400.

4. Whitmore, L. and B. A. Wallace. 2004. DICHROWEB: an online server for protein secondary structure analyses from circular dichroism spectroscopic data. Nucleic Acids Research 32:W668-673.

5. Lobley, A., L. Whitmore and B. A. Wallace. 2002. DICHROWEB: an interactive website for the analysis of protein secondary structure from circular dichroism spectra. Bioinformatics 18: 211-212.

6. Wallace, B., and R. Janes. 2016. Protein Circular Dichroism Data Bank Department of Crystallography, Institute of Structural and Molecular Biology, Birkbeck College, University of London, School of Biological and Chemical Sciences, Queen Mary, University of London, UK.